GA–A23824

ADVANCES IN NOVEL FRC PLASMAS

by
M.J. SCHAFFER, M.R. BROWN, J.A. LEUER, P.B. PARKS,
and C.D. COTHRAN

APRIL 2002

DISCLAIMER

GA–A23824

ADVANCES IN NOVEL FRC PLASMAS

by
M.J. SCHAFFER, M.R. BROWN,† J.A. LEUER, P.B. PARKS,
and C.D. COTHRAN†

This is a preprint of a paper presented at the U.S./Japan Workshop on Physics of Compact Toroid Plasmas, February 25–27, 2002 in Seattle, Washington and to be published in the *Proceedings.*

†Swarthmore College, Swarthmore, Pennsylvania 19081-1397

Work supported by
the U.S. Department of Energy under
Grant No. DE-FG02-00ER54604 and General Atomics IR&D Funds

GA PROJECT 04437
APRIL 2002

ADVANCES IN NOVEL FRC PLASMAS

M.J. Schaffer, M.R. Brown,† J.A. Leuer, P.B. Parks, C.D. Cothran†

General Atomics, P.O. Box 85608, San Diego, California 92186-5608
†Swarthmore College, Swarthmore, Pennsylvania 19081-1397
Schaffer@fusion.gat.com

ABSTRACT

We are studying novel oblate or doublet FRCs that may make desirable fusion reactors. However, their stability and confinement are uncertain and must be understood. Motivated by recent theoretical work showing that weak, axially antisymmetric toroidal magnetic fields are stabilizing, an experiment, SSX–FRC, is being prepared to test this and other ideas. The FRCs will be produced by merging spheromaks. External coils will control the degree of spheromak reconnection and thus the internal toroidal magnetic field. Partially reconnected CTs or doublet CTs can be either FRCs or spheromaks. Both doublet and conventional CTs are investigated with a new Grad-Shafranov equilibrium code. Analytical work shows that FRC rotation may initiate self-generation of the antisymmetric toroidal B. A steady-state D–^{3}He fusion reactor concept is outlined.

INTRODUCTION

Field Reversed Configurations[1] (FRCs) offer notable potential advantages for fusion reactors, especially axisymmetric toroidal plasma confinement at high β ($\beta \sim 1$) in a topology that allows free plasma exhaust and relatively easy maintenance. Furthermore, the high β, low synchrotron emission and unobstructed exhaust stream with direct power conversion might make D-^{3}He fusion reactors possible. High efficiency, high–Q power reactors with long-lived components appear to be more readily attainable with steady-state, rather than pulsed, operation. However, steady-state wall technology sets power density limits and requires larger energy confinement times τ_E than traditional pulsed FRC reactor concepts. Long τ_E requires large values of s ($s = \rho_*^{-1}$ = number of ion gyro-radii contained in the plasma), whereas traditional FRCs have small s. Conventional FRCs are highly prolate,[1] but if radial thermal transport is diffusive, τ_E depends mainly on the square of the shortest distance between the hot core and the cool edge.[2] Thus, approximately-spherical geometry yields the lowest power, most compact steady-state FRC fusion reactors. Therefore, we are investigating relatively short FRCs and their stability, both oblate FRCs and two partially reconected FRCs or doublet FRCs.

No fusion concept based on magnetic plasma confinement is viable without good stability and low anomalous transport. Various MHD and kinetic linear calculations predict the FRC to be unstable to the tilt (m,n) = (1,1) mode except at very low values of s. Nonlinear calculations show unsaturated mode growth and plasma destruction. In stark contrast, experimental FRCs are anomalously stable to the tilt. However, they exhibit large anomalous transport.

Recent theoretical and experimental advances suggest that stable, low-transport-rate FRCs may indeed exist. Numerical studies show stabilization of tilt and shift modes in oblate PRCs by a close fitting conducting shell[3] under conditions also favorable to stabilization of the high (m,n) interchange modes,[4] all in the large-s MHD fluid limit relevant to steady-state. However, oblate FRCs with no nearby wall are not simultaneously stable to both tilt and shift.[3] Furthermore, hybrid simulations (kinetic ions, fluid electrons) reveal near stabilization of the tilt by a combination of spontaneously generated weak toroidal magnetic fluxes and associated strong poloidal ion flows[5] in the absence of a nearby conducting boundary. The toroidal fluxes are generated during the computed FRC formation by the Hall effect, wherein poloidally sheared toroidal electron flow stretches the poloidal field lines of **B** into the toroidal (ϕ) direction.[6,7,5] Figure 1, from Ref. [5], shows that B_ϕ is distributed antisymmetrically (+ and –) in the axial (z) direction with peak values ~30% of the poloidal component B_p. The net toroidal flux is zero. Newer hybrid simulations with additional modes included in the computation show instability of $n > 1$ modes, but they saturate, and a new, lower–s FRC emerges.[8] All the hybrid computations were done without the benefit of a close–fitting conductor.

Recent experiments have scaled up rotating magnetic field (RMF) current drive in a fully ionized FRC plasma.[9] This not only demonstrates one solution to the FRC current drive problem, but unexpectedly, RMF also quiets internal magnetic fluctuations and greatly increases energy and particle confinement times.[10] Improved confinement is also observed in the FIX experiment, where neutral beam injection increases the configuration lifetime.[11]

The predicted tilt stabilization by internal toroidal fluxes leads us to investigate this and other novel FRC plasmas. In this paper we describe modifications to the

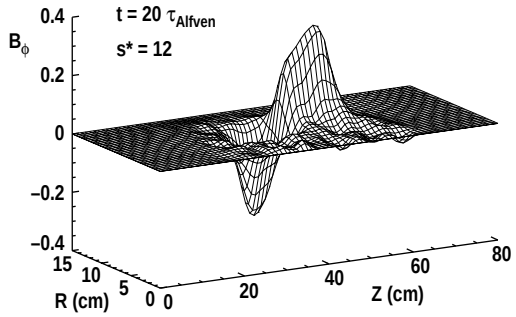

Fig. 1. B_ϕ normalized to the separatrix midplane value of B. Adapted from Ref. [5].

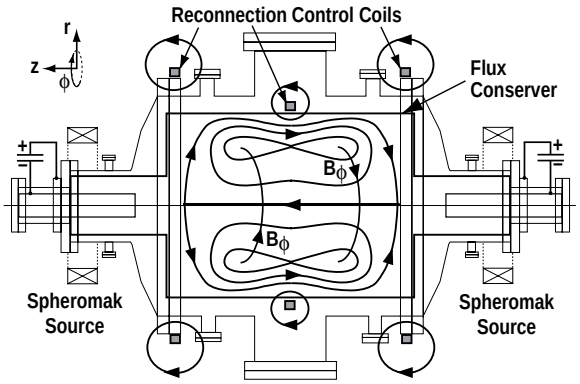

Fig. 2. Schematic of SSX–FRC with reconnection control coils (RCCs) and a new flux conserver.

Swarthmore Spheromak Experiment (SSX)[12] to produce FRCs with central + and – B_ϕ and study their stability in the light of the Ref. [5] hybrid simulations. The FRCs will be formed by partial merging of two counterhelicity spheromaks. Flux from external reconnection control coils (RCCs) will control the extent of spheromak reconnection and thus the residual + and – B_ϕ. The resulting doublet CT configuration has two magnetic axes and an indented equator and is itself a novel configuration. We describe a new finite-element, Grad-Shafranov, free boundary equilibrium code, written to design the SSX RCCs, and we discuss results and conclusions from this code. We show analytically that centrifugal density stratification may initiate antisymmetric B_ϕ growth in a rotating FRC. Since experimental FRCs rotate, spontaneous B_ϕ generation may be ubiquitous, and it may not be necessary to drive B_ϕ from outside. Finally, we outline a D-^{3}He reactor based on a steady-state oblate FRC.

THE SSX–FRC EXPERIMENT

SSX is presently being modified into SSX–FRC, to make FRC plasmas. The merging counterhelicity spheromaks technique, pioneered on TS–3,[13] will be used, but, unlike TS–3, there is no central solid core in SSX–FRC. The modified machine and its operation are illustrated in Fig. 2. The spheromaks are injected into a cylindrical copper flux conserver by two opposing magnetized coaxial guns, one at each end of the conserver. The conserver flux diffusion time is much longer than the plasma lifetime. Flux from external reconnection control coils (RCCs) will be frozen into the conserver to control the extent of spheromak reconnection. As illustrated in the figure, this makes a doublet CT equilibrium with two central private flux regions bounded by a figure-eight separatrix. The opposing spheromak B_ϕ are expected to annihilate in the common flux surrounding the internal separatrix, as during reconnections in TS–3, making an FRC–like plasma confined by B_p alone in that region. Toroidal B is expected to persist inside the unreconnected private regions and leave the residual + and – B_ϕ from the spheromaks in the private regions. SSX-FRC plasmas are expected to have s~5. The CT should have many features of the theoretical B_ϕ-stabilized FRCs.[5] However, the experimental internal B_ϕ will be large (~B_p) rather than weak, at least initially.

The elongation (length/diameter = L_c/D_c) of the SSX–FRC flux conserver, 635 mm/406 mm = 1.56, is deliberately large enough that single-axis CTs are tilt unstable (critical L/D = 0.83 for a single relaxed spheromak), in order to study tilt instability. The equatorial RCC is inside the vacuum chamber in order to be close enough to the plasma to provide the desired shape control. End coils control end geometry, which otherwise is dominated by the fringe field of the gun magnetizing coils. The combined current in the three coils controls the radial gap between the outer separatrix and the conserver. Single-axis FRCs will also be made and investigated. The principle diagnostic for both equilibrium and MHD stability is a set of 600 magnetic probes grouped as 200 three-axis triplets. A Mach probe will measure plasma velocity. Companion papers by M. Brown and C. Cothran in this Workshop give additional information about SSX and SSX–FRC. SSX–FRC will be a flexible facility for FRC research.

NEW CT EQUILIBRIUM CODE AND RESULTS

A new Grad–Shafranov equilibrium solver was written to study SSX–FRC CT equilibria and, in particular, to investigate the sensitivity of the plasma internal flux fraction to the RCC currents and positions.

The Grad–Shafranov equation in the form

$$R\frac{\partial}{\partial R}\left(\frac{1}{R}\frac{\partial \psi}{\partial R}\right)+\frac{\partial^2 \psi}{\partial z^2}=-R^2\mu_o p'-ff'=-\mu_o R J_\phi \quad , \qquad (1)$$

describes static axisymmetric toroidal equilibria. Pressure p and poloidal current f = RB_ϕ are functions of the poloidal flux ψ, and ´ means d/dψ. Eq. (1) is solved using

the finite element partial differential equation tools in Matlab®. The computational domain is bounded by a right circular cylinder flux-conserver, and symmetry is imposed about the midplane. A set of specified current loops impresses a frozen flux into the conserver, and the free boundary solution is determined by solving Eq. (1) by Picard iteration. Iteration begins with a crude initial guess of $J_\phi(R,z)$ and proceeds by solving Eq. (1) for ψ, given the most recent $J_\phi(R,z)$. Then, $J_\phi(R,z)$ is recalculated from this ψ through $p(\psi)$ and $f(\psi)$. At each J_ϕ calculation the scale factors multiplying the p and f profile functions are adjusted to keep the total toroidal plasma current equal to a specified current, I_{plas}. This procedure is simple and well behaved.[14] The code has run on a desktop PC and on desktop and laptop Macintosh® computers.

The code was validated against fixed boundary analytical solutions for a cylindrical Woltjer–Taylor relaxed spheromak ($p = 0$, $f \sim \psi$); a Solovev equilibrium[15] (p' - const., ff' = const.); and a separable cylindrical FRC solution[16] ($p \sim \psi^2$, $f = 0$).

Free boundary equilibria are presently generated by specifying p and f as powers of ψ inside the bounding separatrix (the separatrix is at $\psi = 0$), and $p = f = 0$ in the vacuum region outside it. Separate specifications of p and f inside and outside the internal separatrix are needed to properly represent the SSX–FRC plasmas, which are expected to have $f \approx 0$ outside it and $p' \approx 0$ inside it. However, this capability is not yet implemented.

Figure 3 shows an example of two partially merged doublet CT equilibria calculated in the SSX–FRC flux conserver with frozen fluxes produced by four RCCs. The end coils are located as shown in Fig. 2, but the equatorial coil is split into two coils in Fig. 3 to allow radial diagnostic access between them. These FRC equilibria have moderately peaked pressure profiles, $p \sim \psi^{1.5}$, and $f = 0$. Both equilibria have $I_{plas} = 100$ kA. They differ only in the current in the equatorial loops used to establish the frozen flux, 8 kA (in two coils) in the first case and 13 kA in the second. Each end coil carries 1.3 kA. The midplane coil current in the first case lets 84% of the poloidal flux reconnect, but the higher current in the second case lets only 46% reconnect. Therefore, the RCCs can regulate the degree of equilibrium reconnection. Two-dimensional evolution of the reconnection has been studied by TRIM simulations.[17] Stability of these equilibria will be studied in the future.

For more peaked pressure profiles, $p \sim \psi^2$, the equilibria change rapidly between weakly reconnected and highly reconnected while the equatorial flux-setting coil current(s) vary only slightly, indicating that it may be more difficult to control reconnecting CTs having peaked

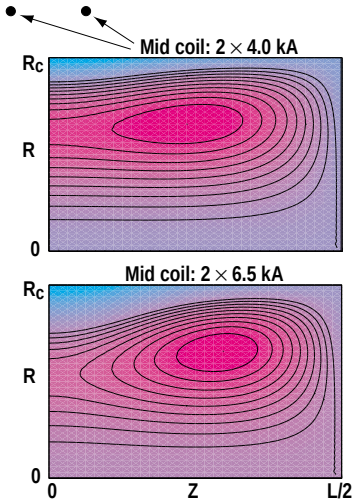

Fig. 3. Computed partially reconnected FRC equilibria in the SSX–FRC flux conserver. Only half of an equilibrium is plotted. Locations of two current loops, representing a split equatorial coil, are indicated in the top figure. Only the equatorial coil currents differ, and the reconnected fluxes are 84% (top) and 46% (bottom).

pressure profiles. For slightly less peaked profiles, $p \sim \psi^{1.75}$, the reconnected flux fraction depends reasonably on the equatorial coil current, and reconnection control becomes progressively less sensitive as the pressure profile peaking exponent is decreased. It is not yet known what pressure profiles will be produced in SSX–FRC. Conventionally formed FRCs have broad pressure profiles, and they usually have hollow current profiles. Such plasmas would be easy to shape using externally applied magnetic fluxes.

Conventional single-axis elongated FRC equilibria in a long cylindrical flux conserver have also been calculated. Figure 4 shows two equilibria from a sequence with increasing I_{plas}. All are inside a flux conserver, (L_C/D_C) = (2 m/0.4 m) containing an initial uniform 1 T magnetic induction. All have $p \sim \psi$. The FRC midplane separatrix radius R_S remains nearly constant while the separatrix length L_S increases almost linearly with increasing I_{plas}, except for very short or very long (near the conducting end plate) plasmas. The ratio $x_S = R_S/R_C$ is 0.825 in the linear L_S/I_{plas} regime. This is in good agreement with the analytic condition for axial equilibrium,[18,19] $x_S = [2(1 - \beta_x)]^{1/2} = (2/3)^{1/2} \approx .8165$, where the midplane cross-section-averaged beta, β_x, is 2/3 for $p \sim \psi$.

Figure 5 shows two equilibria with peaked profiles, $p \sim \psi^2$. Here L_S, grows only weakly with increasing I_{plas}, even though I_{plas} spans a range of 30/2. This is understood in terms of axial equilibrium. For $p \sim \psi^2$ the analytic β_x is 1/2 for high elongation, so axial equilibrium

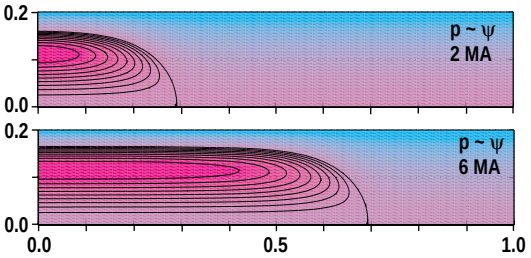

Fig. 4. Computed FRC equilibria in a long cylindrical flux conserver, for $p \sim \psi$ and two values of I_{plas}.

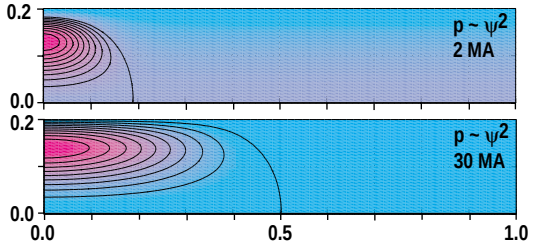

Fig. 5. Computed FRC equilibria in a long cylindrical flux conserver, for $p \sim \psi^2$ and two values of I_{plas}.

requires $x_s = 1$. Higher I_{plas} mainly increases the magnitude of B, in order to compress the constant vacuum flux ever more tightly against the conserver to drive x_s toward unity. Profiles more peaked than $p \sim \psi^2$ have $\beta_x < 1/2$ and do not elongate, because the plasma pressure cannot overcome the axial magnetic tension.

DOUBLET CT

The doublet CT, with or without internal B_ϕ, is a novel plasma configuration. Little is known yet how it will behave. Here we discuss interchange stability qualitatively. Interchange instability is driven by ∇p with bad curvature. In the absence of B_ϕ, each magnetic line closes on itself, and plasma compressibility and good curvature are the only stabilizing effects. Near the bounding separatrix, average curvature is bad, but flux tube specific volume decreases rapidly inward, providing stabilization by compressibility. This is the same as in conventional FRCs.[4] Just outside the figure-eight separatrix the average curvature is good and is stabilizing. Inside the private regions average curvature is again bad, but specific volume variation again gives compressibilty stabilization. There is a surface in the common region where neither curvature nor compressibility stabilize the mode, so the pressure gradient might be low there. Doublet CTs will be studied experimentally in SSX–FRC.

SELF B_ϕ GENERATION IN ROTATING FRCS

Toroidal magnetic field may be desirable in FRCs for stability, as argued in the Introduction. In this Section we demonstrate two two-fluid mechanisms, radial density gradient and Hall effect, by which centrifugal density stratification in a toroidally rotating FRC might drive anti-symmetric $\partial B_\phi/\partial t$. Here we do not calculate a final steady state B_ϕ but just show terms that contribute to $\partial B_\phi/\partial t = -\nabla\times\mathbf{E} \neq 0$ in a steadily rotating stationary FRC equilibrium that starts with only B_p. The electric field is calculated from the electron momentum or Ohm's law, giving

$$\partial B_\phi \big/ \partial t = -\hat{\mathbf{e}}_\phi \cdot \left(\nabla \times \mathbf{E}\right) = \hat{\mathbf{e}}_\phi \cdot \nabla \times \left[\left(\nabla p_e - \mathbf{J}_e \times \mathbf{B}\right)\big/ en\right]. \quad (2)$$

Subscripts e and i identify electron and ion, respectively, $n = n_e = Zn_i$, $\mathbf{J}_e = -env_e$, $p_e = n_eT_e$ and $\hat{\mathbf{e}}$ is a unit vector. Thermal force terms are not analyzed in this paper. Coordinate systems are cylindrical (R,ϕ,z) or flux surface based (x_n,x_p,ϕ), where $\hat{\mathbf{e}}_n$ = outward normal to the magnetic surface and $\hat{\mathbf{e}}_p$ = poloidally tangent to it. Poloidal flux ψ is an alternate normal coordinate, with $\psi(R=0) = 0$. For right handed coordinate systems, $d\psi = -RB_p\, dx_n$, $\nabla\psi = -RB_p\, \hat{\mathbf{e}}_n$ and ψ is positive in the CT if B_p is positive. T_e and T_i are nearly constant on a closed magnetic surface and so are functions of ψ only. Density and pressures are functions of (ψ,R) or equivalently of (ψ,x_p). Neither p_e nor p_i are constant on a magnetic surface in rotating plasmas.

The first right side term of Eq. (2), the "density gradient" term, becomes

$$\left.\frac{\partial B_\phi}{\partial t}\right|_{\nabla n} = \frac{\nabla T_e \times \nabla \ln n}{e} \cdot \hat{\mathbf{e}}_\phi = -\frac{dT_e}{ed\psi} R\mathbf{B}_p \cdot \nabla \ln n \quad . \quad (3)$$

The second or "Hall" term becomes

$$\left.\frac{\partial B_\phi}{\partial t}\right|_{Hall} = \left(\nabla\Omega_e \times \nabla\psi\right) \cdot \hat{\mathbf{e}}_\phi = R\mathbf{B}_p \cdot \nabla\Omega_e \quad , \quad (4)$$

where $\Omega_e = v_e/R$ is the electron toroidal angular rotation frequency. Eq. (3) is nonzero only if the density and temperature gradients are not aligned. This is possible if $n(\psi,R)$ acquires a centrifugal radial gradient from rotation. In Eq. (4), $\Omega_e(\psi,R)$ acquires shear in the magnetic surface from the increased equilibrium J_ϕ driven at large R by the outward centrifugal pressure. Since the electrons are tied to the magnetic lines, sheared Ω_e stretches poloidal magnetic lines into the toroidal direction.[6]

Figure 6 illustrates the vectors contributing to the density gradient and Hall terms. Both mechanisms operate maximally at the axial extremes of the magnetic surfaces, and both generate $\partial B_\phi/\partial t$ of opposite signs at opposite ends. The sign of $\nabla\Omega_e$ corresponds to a steadily rotating axisymnetric equilibrium obtained by Hinton and Wong.[20] In this equilibrium, the two mechanisms oppose and cancel each other, because of $\nabla\times\mathbf{E} = 0$ is imposed.

It is straightforward to calculate the density gradient effect, Eq. (3). In a rotating equilibrium with isothermal magnetic surfaces, the density and its gradient are[20]

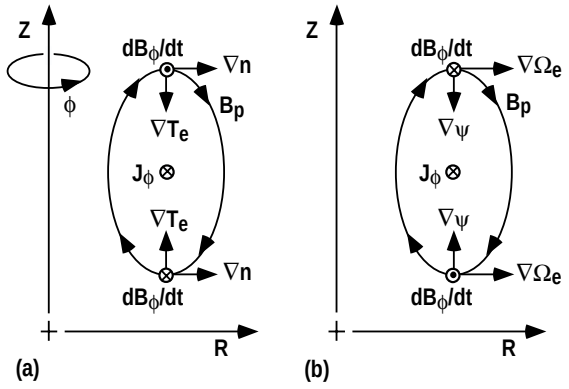

Fig. 6. Vectors from eqs. (3) and (4) contributing to the density gradient (a) and the Hall (b) B_ϕ generation .

$$n(\psi,R) \approx N(\psi)\exp\left[m_i\Omega_i^2\left(R^2 - R_{ref}^2\right)\Big/2ZT\right] \text{ and} \qquad (5)$$

$$\nabla \ln n(\psi,R) \approx (\partial n/\partial\psi)\nabla\psi + \left(m_i\Omega_i^2 R/ZT\right)\hat{\mathbf{e}}_R \quad . \qquad (6)$$

The $\nabla\psi$ term does not contribute to Eq. (3), leaving

$$\left.\frac{\partial B_\phi}{\partial t}\right|_{\nabla n} = -\frac{m_i\Omega_i^2 R^2}{eZT}\frac{dT_e}{d\psi}\left(\mathbf{B}_p\cdot\hat{e}_R\right) \quad . \qquad (7)$$

The rate of B_ϕ growth depends mainly on Ω_i^2, since $(R\nabla T_e)/T \sim 1$. For $\Omega_i \sim 10^5\ s^{-1}$ in typical FRCs and $m_i/eZ \sim 10^{-8}$ kg/C, this yields $\partial B_\phi/\partial t \sim 100$ T/s, or 0.1 T/ms. This is somewhat less than the rate of typical FRC B_p decay. It is instructive to normalize $\partial B_\phi/\partial t$ by B_p/τ_{ref}, where τ_{ref} is some characteristic time. Define $\gamma = (\partial B_\phi/\partial t)/B_p$. If $\tau_{ref} = 1/\Omega_i$, then

$$\gamma/\Omega_i = M_{th}\left(\rho_{ci}/L_{Te}\right)\left(T_e/T\right) \quad , \qquad (8)$$

where $M_{th} = v_{i\phi}/v_{ith}$, v_{ith} = ion thermal velocity, ρ_{ci} = ion gyro radius and $L_{Te} = T_e/|\nabla T_e|$. While both ρ_{ci} and L_{Te} should be evaluated at the axial extremes of the magnetic surface, the ratio $\rho_{ci}/L_{Te} \sim 1/s$ is insensitive to where it is evaluated. Eq. (8) shows that it takes more plasma revolutions to build B_ϕ to $\sim B_p$ as s increases. If instead we choose $\tau_{ref} = \tau_A = L_A/v_A$, where v_A = Alfvén speed and L_A = the length used to define the Alfvén time, then

$$\gamma/\tau_A = M_A^2\left(\left(c/\omega_{pi}\right)/R\right)\left(L_A/L_{Te}\right)\left(T_e/T\right) \quad , \qquad (9)$$

where

$$M_A^2 = \left(\Omega_i R/v_A\right)^2 = m_i n_i \Omega_i^2 R^2\Big/\left(B_p^2/\mu_o\right) = \beta_{rot} \qquad (10)$$

and $\left(c/\omega_{pi}\right)/R = 1/S_* \approx 0.1/s$. The Alfvén time is the time scale for the growth of MHD instabilities like the tilt mode. Therefore, unless the FRC is rotating at near Alfvénic speed and has low s, it will be necessary to supply an initial B_ϕ, if B_ϕ is necessary for MHD stability. An oblate FRC surrounded by a nearby stabilizing conducting wall might avoid this requirement, however.

It is difficult to predict how the poloidal shear of **J** divides between Ω_e and Ω_i in the general case and, therefore, how it might contribute to toroidal B generation. However, as an example, if Ω_i were to not vary within a magnetic surface, then all the poloidal shear of **J** would necessarily appear in Ω_e. Then

$$\left.\frac{\partial B_\phi}{\partial t}\right|_{Hall} = -\frac{m_i\Omega_i^2 R^2}{eZ}\frac{d\ln\left(\Omega_i^2 R_0^2/T\right)}{d\psi}\left(\mathbf{B}_p\cdot\mathbf{e}_R\right) \qquad (11)$$

where R_0 is any fixed characteristic radius. The sign of this contribution would depend on the shear from surface to surface of $\ln\left(\Omega_i^2 R_0^2/T\right)$, which is proportional to ln (M_{th}). Alternatively, the Ω_e shear could be imposed by an external current drive means.

OBLATE FRC D-^{3}He FUSION REACTOR

A spherical geometry was chosen for reasons stated in the Introduction. A conceptual design, developed to illustrate the scale of a steady-state D-^{3}He FRC reactor is summarized here. Figure 7 is a sketch of a conceptual steady state, oblate FRC fusion reactor. The FRC plasma is confined by poloidal magnetic field produced by circular superconducting coils. A 0.9 m-thick shield limits coil heating by neutrons emitted by minority DD and DT fusion in the plasma. Current drive must be provided at the magnetic axis by means as yet untested at relevant conditions. Bremsstrahlung radiation power is absorbed in the first wall and can be converted by a thermal cycle. Synchrotron power, though low for an advanced fuel magnetically confined plasma, must still be highly reflected and absorbed in the plasma to ignite. Plasma diffusing into the scrape-off layer (SOL) carries the majority of the fusion power. In principle it can converted to electricity by a direct converter. The fusion power of this design is 2 GW, chosen arbitrarily. The Table lists some major parameters.

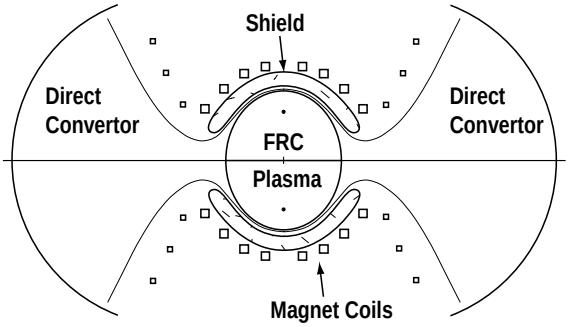

Fig. 7. Oblate FRC steady-state fusion reactor.

Table 1: FRC Fusion Reactor and Plasma Parameters

Fuel (specified)	50 D, 50 ^{3}He
Central temperature (specified)	100 keV
Fusion power (specified)	2 GW
First wall thermal power (specified)	10 MW/m^2
Plasma average radius	1.74 m
Plasma volume	22 m^3
Plasma internal energy	1.1 GJ
Central plasma pressure	69 MPa
Average magnetic field at coil	9.4 T
Central ion density, D + ^{3}He	$17 \cdot 10^{20}$ m^{-3}
Central electron density	$26 \cdot 10^{20}$ m^{-3}
Plasma current	32 MA
Required energy confinement time	0.7 s
Number of contained ion gyroradii	~75

The required energy confinement time given in Table 1 is the minimum value consistent with having 1.1 GJ of plasma internal energy, 2 GW of fusion power and 0.46 GW of radiated power. A τ_E of ~0.7 s in a plasma of this size is on a par with advanced tokamak confinement. At present it is not known if FRC confinement can be this high. Therefore, research into the inherent limits of FRC confinement is crucial to the viability of the steady-state oblate D-^{3}He FRC reactor.

CONCLUSION

The high β of field reversed configurations (FRCs) and their unlinked magnet topology might make possible a steady-state D-^{3}He fusion power core. However, excellent plasma stability and confinement are required. Theory suggests that short FRCs, such as wall stabilized oblate FRCs or doublet-FRCs, might offer improved stability. Interchange and ballooning modes in FRCs and dipole fields[21] share many features and can be profitably studied together. Rotating FRCs might generate steady-state toroidal magnetic fluxes. Continued and expanded FRC experiments and theory are urgently needed to provide a firm physics basis for this and other FRC concepts.

ACKNOWLEDGMENT

Work supported by U.S. Department of Energy Grant DE-FG02-00ER54604 and General Atomics IR&D funds.

REFERENCES

[1]M. Tuszewski, Nucl. Fusion **28** (1988) 2033.

[2]S.P. Auerbach, W.C. Condit, Nucl. Fusion **21** (1981) 927.

[3]E.V. Belova et al., Phys. Plas. **8** (2001) 1267.

[4]L. Sparks et al., Phys. Fluids **23** (1980) 611.

[5]Yu. Omelchenko, Phys. Plas. **7** (2000) 1443.

[6]D.W. Hewett, Nucl. Fusion **24** (1984) 349.

[7]R.D. Milroy, Phys. Fluids **29** (1986) 1184.

[8]Y.A. Omelchenko, Phys. Plas. **8** (2001) 4463.

[9]J.T. Slough, K.E. Miller, Phys. Plas. **7** (2000) 1945.

[10]J.T. Slough et al., Phys. Rev. Lett. **85** (2000) 1444.

[11]T Asai et al., Phys. Plas. **7** (2000) 2294.

[12]C.G.R. Geddes et al., Phys. Plas. **5**, (1998) 1027.

[13]Y. Ono et al., Phys. Fluids B **5** (1993) 3691.

[14]D.W Hewett, RL Spencer, Phys. Fl. **26** (1983) 1299.

[15]L.S. Solovev, Sov. Phys. JETP **26** (1968) 400.

[16]P.B. Parks, in preparation (2002).

[17]V.S. Lukin et al., Phys. Plas. **8** (2001) 1600. M.R. Brown et al., this Workshop (2001).

[18]W.T. Armstrong et al., Phys. Fluids **24** (1981) 2068.

[19]V.N. Semenov, N.V. Sosnin, Sov. J. Plas. Phys. **7** (1981) 180.

[20]F.L. Hinton, S.K Wong, Phys.Fluids **28** (1985) 3082.

[21]J. Kesner et al., Nucl. Fusion **41** (2001) 301.